



46th SME North American Manufacturing Research Conference, NAMRC 46, Texas, USA

## “Performance Comparison of Sol-gel with White Alumina Abrasives for Grinding of Super Duplex Stainless Steel (SDSS)”

D. Selvakumaran<sup>a</sup>, N. Arunachalam<sup>b</sup>, L. Vijayaraghavan<sup>c\*</sup>, A.S.S. Balan<sup>d</sup>

<sup>a</sup>M.S. Research Scholar, Department of Mechanical Engineering, Indian Institute of Technology Madras, Chennai, India

<sup>b</sup>Assistant Professor, Department of Mechanical Engineering, Indian Institute of Technology Madras, Chennai, India

<sup>c</sup>Professor, Department of Mechanical Engineering, Indian Institute of Technology Madras, Chennai, India

<sup>d</sup>Associate Professor, Department of Mechanical Engineering, Vellore Institute of Technology, Vellore, India

\* Corresponding author. Tel.: +91-44-2257-4687; fax: +91-44-2257-4652.

E-mail address: [lvijay@iitm.ac.in](mailto:lvijay@iitm.ac.in)

---

### Abstract

Super duplex stainless steel (SDSS) serves different applications in industry categories like oil and gas, offshore platforms, naval, nuclear, pharmaceutical, mining, etc. due to its high strength, resistance to pitting and stress corrosion cracking properties. The two-phase microstructure of SDSS along with the other alloying elements makes this a difficult-to-machine material. The above-mentioned applications require finished components with good dimensional accuracy and surface finish. Traditionally, grinding process is used as a final machining process to achieve the prescribed tolerance requirements. In the current industrial practice, the grinding wheel with fused white alumina grains is most widely used for finishing of ferrous components. In spite of its acceptance in industries, there is a need for an abrasive grain with extended redress life for grinding a wide variety of steel grades. To cater for this requirement, sol-gel alumina abrasive grains were introduced which has a prolonged redress life due to its high fracture toughness characteristics. In this paper, the performance of the sol-gel alumina grinding wheel is compared with the white alumina wheel for grinding of SDSS material. To compare the performances of both the grinding wheels, indices such as grinding force, specific grinding energy, surface roughness, grinding ratio, and grinding efficiency were calculated based on the experimental work. The results obtained indicate that grinding wheel with sol-gel alumina grains performed better than the fused white alumina grains.

© 2018 The Authors. Published by Elsevier B.V.

Peer-review under responsibility of the scientific committee of the 46th SME North American Manufacturing Research Conference.

*Keywords:* Grinding Process; Sol-gel alumina; Grinding Wheel wear; Cutting forces; Grinding efficiency

---

## 1. Introduction

Super duplex stainless steel materials (SDSS) are best suited for robust applications in heavy engineering industries due to their excellent mechanical and corrosion resistance properties. The dual phase with almost balanced austenitic-ferrite microstructures makes this a unique material. In order to meet specific application requirements, the finishing of this material in a different form is very much essential. Grinding is a most widely used finishing process to achieve the required surface integrity and dimensional accuracy of the workpiece [1]. The unique phase and microstructure of SDSS material call for an alternate grinding wheel abrasive grains for high performance grinding in comparison with traditional white alumina wheel. Apart from the material requirement, there is a need for an eco-friendly and energy efficient grinding process. This necessitates the need for abrasive grains that can resist the wear and have an extended redressing time through an adequate friable property. The grinding wheel requires frequent dressing which lowers the productivity and increases the material cost. Traditionally, the alumina wheels are the most preferred ones for grinding of wide variety and grade of steels as they possess controlled wheel porosity and structure in vitreous bonds.

The industrial acceptance of this sintered alumina grains is lagging behind the fused white alumina grains due to its cost of production. From the sustainability point of view, there is a need for a more efficient grinding process. In this regard, this research directed towards identifying abrasive grains with extended dressing intervals. Krell et al., [2] compared microstructure and mechanical properties of various grades of sintered alumina grains with fused white alumina grains. This study revealed the increased toughness and grinding efficiency of sintered grains. Yoon and Krueger [3] evaluated and compared the performance of the sol-gel grinding wheel and a conventional grinding wheel under different cutting fluids for two different grades of steel. The sol-gel alumina grinding wheels with a synthetic emulsion containing extreme pressure lubricants (EP) on a grinder with typical stiffness gave better performance.

Klocke et al., [4] evaluated the wear mechanism of Sol-gel abrasive grains using single grit scratch test. The severe plastic deformation and the crack bridging contributed to the wear of the Sol-gel abrasives. Also, the improved tribological behavior of these abrasive grains was due to the presence of surface oxide layer.

Eduardo Carlos et al., [5] compared the performance of alumina wheel and cBN wheel by calculating the cutting force, surface roughness, wheel wear and the Grinding ratio (G-ratio). Though a lower value of cutting force and better surface finish were obtained from conventional grinding wheel due to the dressing operation, cBN wheel gives a higher G-ratio. From this, the conventional grinding wheel was found to be appropriate for rough and finishing operation for obtaining a good surface finish. Mayer et al., [6] investigated the wear mechanism of nano-metric scale commercial Sol-gel corundum. The results indicate that the combined effect of controlled sub-surface shear cracks and plastic deformation leads to the formation of flat zones in the grains. On these contact zone, nano-crystalline FeO debris layer adheres to the alumina grains which leads to an improved tribological performance.

Manimaran et al., [7] used a sol-gel alumina grinding wheel on an AISI 316 stainless steel workpiece and compared its performance under dry, wet and cryogenic coolant conditions. Cryogenic coolant provided better lubrication by reducing the grinding force, improving the surface finish and produced fewer defects compared to dry and wet cooling conditions. The effects of liquid nitrogen delivery pressure on the machining zone in terms of surface roughness, grinding force and temperature were also studied. Nadolny [8] discussed the production methods, properties, and application of Sol-gel abrasive grains along with white alumina grains and cBN grains. The results indicate that the Sol-gels grains with microcrystalline structure offer an extended period between dressing cuts with increased material removal rate. Nadolny [9] evaluated the role of the bond volume on the wear phenomenon of the microcrystalline sintered corundum abrasive grains and the ceramic bond bridges with glass-crystalline structure. The results indicated that the decrease in bond volume increased the grinding wheel life. This was due to a decrease in abrasive wear, plastic flow, and greater fracture wear. Rajaguru and Arunachalam [10] evaluated the suitability of the different coated tools for machining of SDSS under dry turning conditions. The material requires an investigation on its grindability with a properly chosen abrasive grains for a grinding wheel. In this work, the performance of a sol-gel based alumina grinding wheel sintered at 1120°C was compared with the white alumina wheel

by assessing the wheel loading, grinding forces, surface finish, specific cutting energy, grinding ratio, and grinding efficiency.

## 2. Material and Methods

The SDSS material of grade 2507 is used in this study, which has an almost equal proportion of ferrite and austenite. The microstructure of the material used in this study is shown in Fig.1. The ultimate tensile strength of the material is 910 MPa with a Rockwell hardness of 32 HRC. The elemental composition of the material is given in Table 1.

Table 1. Chemical composition of SDSS.

Element	C	N	Si	P	S	Cr	Mn	Ni	Mo	Fe
Wt(%)	0.03	0.25	2.06	0.03	0.02	24.06	1.20	6.1	4	Bal.

The experiments were conducted on SDSS material having a size of (30×30×20 mm). The tests were carried out with two types of grinding wheels namely,

- Sol-gel alumina-based grinding wheel sintered at 1120°C.
- White alumina grinding wheel.

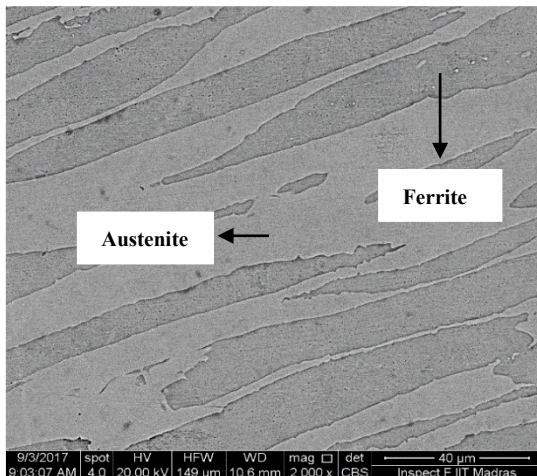


Fig. 1. Microstructure of SDSS material.

The specifications of both the grinding wheels are Provided in Table 2.

Table 2. General Characteristics of grinding wheels.

Short name	Al <sub>2</sub> O <sub>3</sub> grinding wheel	Sol-gel grinding wheel
Technical designation of wheel	AA60K5V8	SG60K5V8
Grinding wheel type		Straight grinding wheel
Volume of abrasives (%)	48	50
Volume of bond (%)	15	16
Volume of pores (%)	37	34
Dimensions		External diameter = 180 mm Bore diameter = 31.75 mm Width = 13 mm

Experiments were performed on Chevalier model smart H-B81-8II grinding machine. Reciprocating type of grinding was performed. The experiments were conducted under flooded cooling condition. The emulsion used was KYROS EPSOL Super S1-emulsion (concentration of the emulsion: 5% of soluble oil and remaining water). The flow rate of the coolant was maintained constant at 60 liters/hr. with a pressure of 1 bar. A selected infeed was given at the end of the stroke and each experiment was performed for ten passes. Experiments were designed based on a full factorial design with 4 levels for grinding wheel speed and radial depth of cut respectively. The first set of experiments were conducted to study the influence of process parameters on the performance indices. The experiments were repeated twice for estimating the uncertainty of the results. Although the properties such as hardness and ductility were similar for both the wheels, the sol-gel alumina wheel possessed a higher number of micro grains with uniform shape and size. The characteristics of both the grains are shown in Table 3. The experimental setup is shown in Fig.2.

Table 3. General Characteristics of grain.

Product characteristics	Azures-II	Alumina
Grain Size (μm)	60	60
Specific gravity ( g/cm <sup>3</sup> )	3.96	4.1
Color	Blue	White
Hardness (HV(Kgf/mm <sup>2</sup> ))	2300-2600	2000-2200
Fracture toughness, MPa. m <sup>1/2</sup>	3.9 - 4.3	3.5
Melting point (°C)	2050	2072

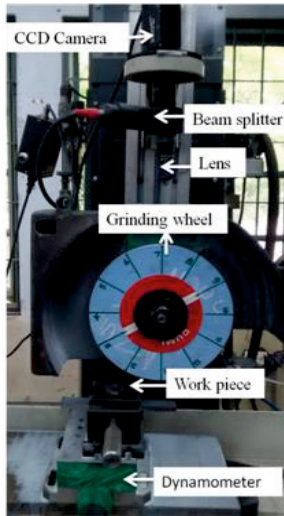


Fig. 2. Photograph of experimental setup

The process conditions used for the experimental work is given in Table 4.

Table 4. General data of grinding conditions

Parameter	Description
Cutting velocity ( $V_c$ )	20 m/s, 22 m/s, 24 m/s, and 26 m/s.
Radial depth of cut ( $a_c$ )	4 $\mu\text{m}$ , 8 $\mu\text{m}$ , 12 $\mu\text{m}$ , and 16 $\mu\text{m}$ .
Grinding wheel	Sol-gel alumina and $\text{Al}_2\text{O}_3$ grinding wheel.
Workpiece materials	Super duplex stainless steel-2507 (32 HRC)
Type of pre-dressing condition	Single point flat dressing with a radial depth of cut of 10 $\mu\text{m}$ , cross feed of 100mm/min and Grind wheel speed 20 m/s
Type of grinding	Wet grinding
Wheel width (b)	13 mm

The second set of experiments was conducted with selected grinding conditions to evaluate the G-ratio, grinding forces and the grinding efficiency to compare the performances of the grinding wheels. The normal and the tangential forces were measured during the tenth pass for each experiment and are used to obtain the average grinding forces. The Kistler make 9257-B dynamometer with an NI-9215 data acquisition system

was used to collect the grinding force data for further analysis. The surface roughness of the workpiece was measured using a non-contact 3D surface profiler. The grinding wheel images were taken at multiple locations using a Basler make CCD camera with a resolution of 1024 x 1024 pixels to evaluate the grinding wheel loading at different conditions and with a different number of passes. The captured images were analyzed using a region growing segmentation technique to find out the wheel loading in percentage [11]. To evaluate the G-ratio, a part of the grinding wheel was used for the grinding operation for 1000 passes and then the step size was measured using a CMM to measure the radial wear of the grinding wheel. Using this volume of material removed calculated for the grinding wheel. The ratio between the volumes of material removed from the grinding wheel to the workpiece calculated to get G-ratio. The process outcomes were evaluated to compare the grinding performance of the sol-gel with the white alumina wheel.

### 3. Results and Discussion

#### 3.1. Grinding forces

The effect of parameters on the tangential force and the normal force for the two grinding wheels are shown in Fig. 3 (a), (b) and Fig. 4 (a), (b) respectively. When the cutting velocity increases, there is a reduction in both the tangential and the normal forces. This can be attributed to the fact that the undeformed chip thickness reduces at higher cutting velocity. In addition, it is also observed that the grinding forces increase with increase in the radial depth of cut. This may be due to the increase in the wheel loading and the undeformed chip thickness at a higher radial depth of cut. Sol-gel wheel possesses lower order grinding force when compared to the aluminum oxide wheel due to the size of the average crystal of the sol-gel abrasives being in sub-micrometer range. These sol-gel abrasives have a microfracture capability with high fracture toughness, contributed for a lower order grinding force.

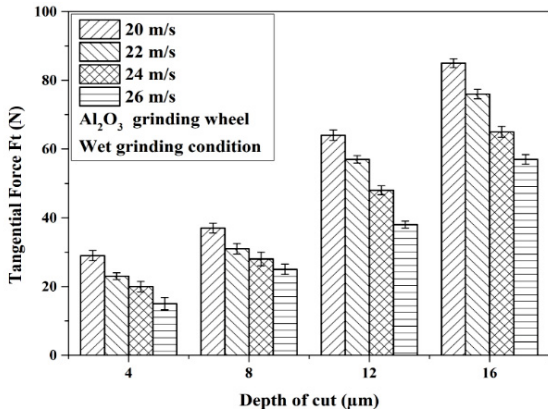


Fig. 3. (a) Variation of tangential force with process parameters for the Al<sub>2</sub>O<sub>3</sub> wheel.

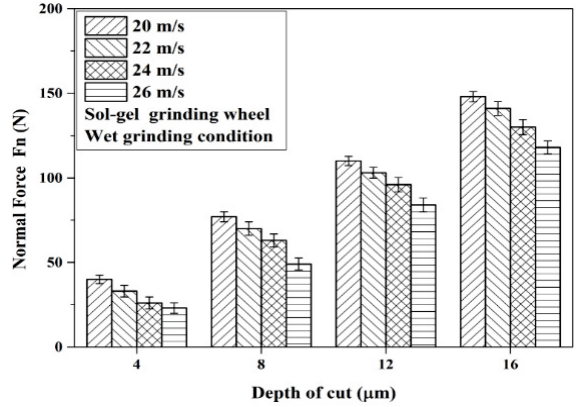


Fig. 4. (b) Variation of normal force with process parameters for sol-gel wheel

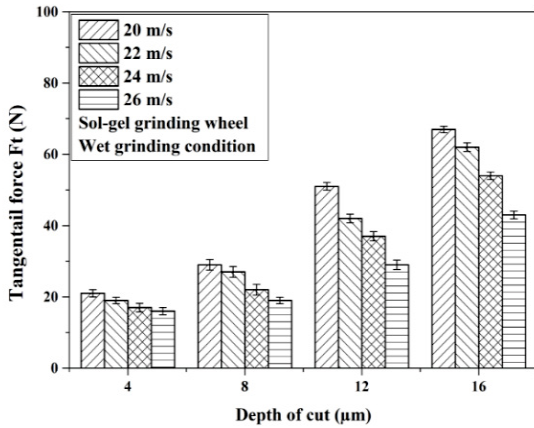


Fig. 3. (b) Variation of tangential force with process parameters for sol-gel wheel

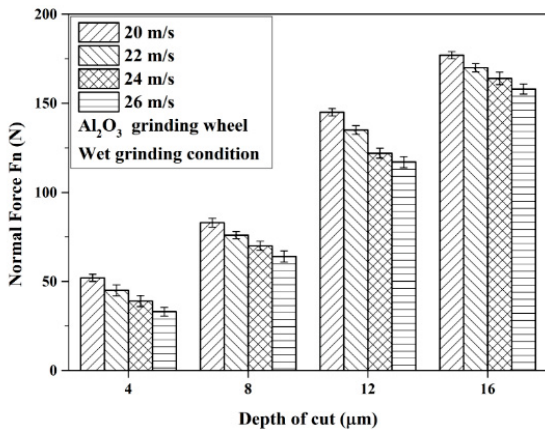


Fig. 4. (a) Variation of normal force with process parameters for Al<sub>2</sub>O<sub>3</sub> wheel.

### 3.2 Grinding wheel loading

The loading of the grinding wheel was evaluated using the optical images captured after each experiment. The region growing segmentation technique was used to analyze the images and evaluate the percentage of wheel loading. The images for both the grinding wheels before and after the segmentation are shown in Fig. 5 (a), (b) and Fig. 6 (a), (b).

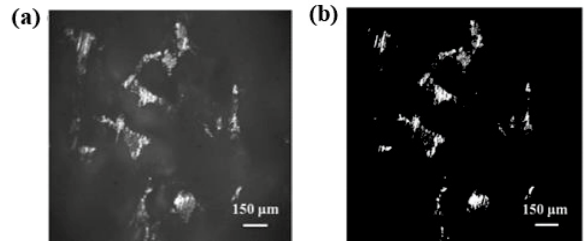


Fig. 5. (a) Wheel surface in the loaded condition before segmentation and (b) Shows the wheel surface after segmentation of Al<sub>2</sub>O<sub>3</sub> grinding wheel images under ( $V_c = 26$  m/s,  $a_e = 16$  μm).

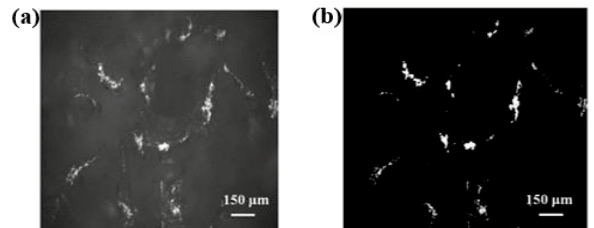


Fig. 6. (a) Wheel surface in the loaded condition before segmentation and (b) Shows the wheel surface after segmentation of sol-gel grinding wheel images under ( $V_c = 26$  m/s,  $a_e = 16$  μm).

From Fig.7. (a), it is observed that the wheel loading increases with increase in the radial depth of cut for the Al<sub>2</sub>O<sub>3</sub> wheel. This is due to the fact that the chips get adhered to the grains at a higher radial depth of cut. From Fig.7. (b), it is observed that the increased hardness of the sol-gel grinding wheel sintered at a higher temperature does not allow the metal particles to settle in the pores of the abrasive grains in the grinding wheel.

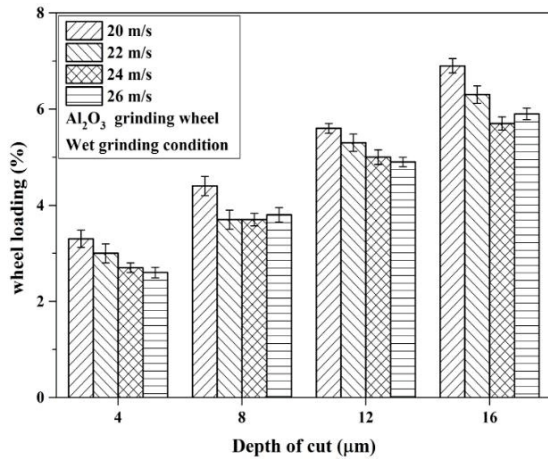


Fig. 7. (a) Variation of wheel loading (%) with process parameters for the Al<sub>2</sub>O<sub>3</sub> wheel.

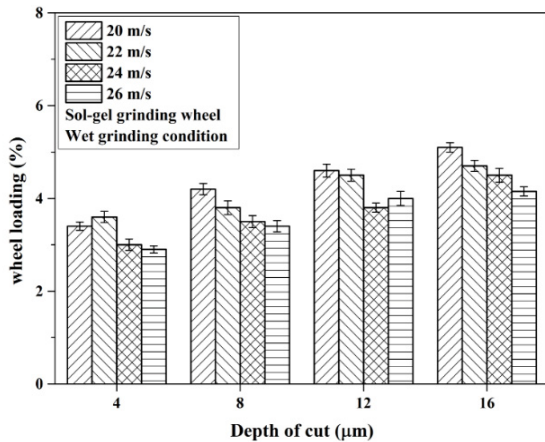


Fig. 7. (b) Variation of wheel loading (%) with process parameters for the sol-gel wheel.

### 3.3 Surface roughness

Typical monitored parametric influence on the roughness of ground SDSS surface with different grinding wheels are illustrated in Fig.8 (a), (b).

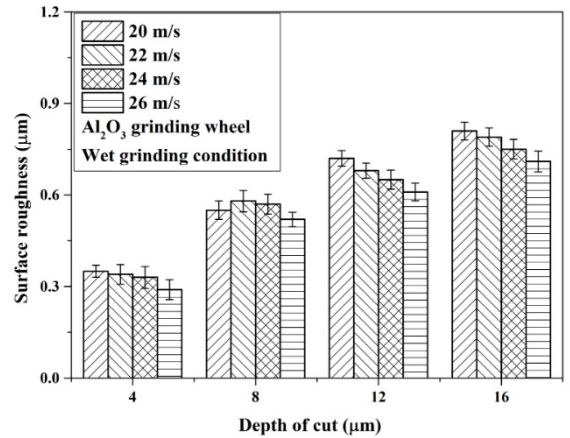


Fig. 8. (a) Variation of surface roughness with various process parameters for the Al<sub>2</sub>O<sub>3</sub> wheel.

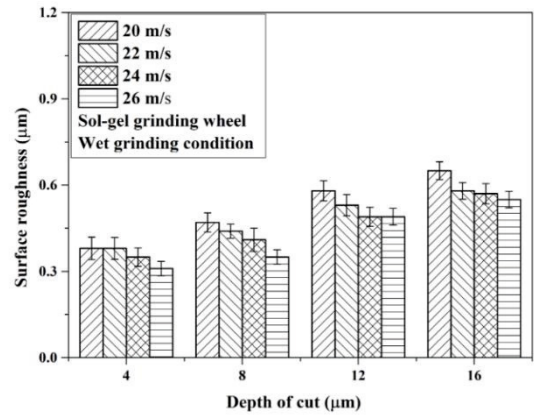


Fig. 8. (b) Variation of surface roughness with process parameters for the sol-gel wheel.

It is observed that there is a reduction in the surface roughness with an increase in cutting speed for a constant radial depth of cut. The fluctuation in surface roughness along with error bar is plotted for each case. There are no significant changes in the surface roughness values were observed as the order of variation of cutting velocity is smaller. The surface roughness obtained by the sintered sol-gel abrasives was better in all the grinding conditions due to the increased sliding action of grains with the workpiece.

This is due to the controlled sub-surface shear cracks and plastic deformation leads to the formation of flat zones in the grains [6].

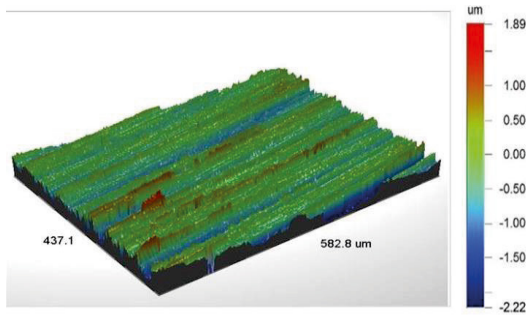


Fig. 9. (a) 3D Surface profile of Super duplex stainless steel ground using Al<sub>2</sub>O<sub>3</sub> ( $V_c = 22$  m/s,  $a_e = 8$   $\mu$ m)

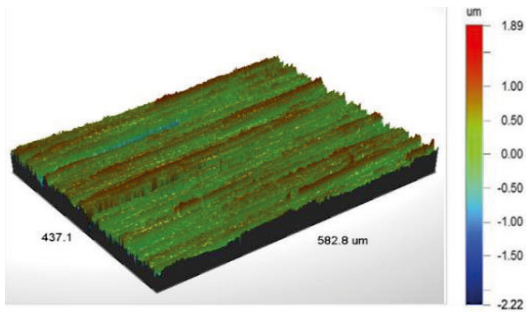


Fig. 9. (b) 3D Surface profile of Super duplex stainless steel ground using sol-gel ( $V_c = 22$  m/s,  $a_e = 8$   $\mu$ m)

### 3.4 Specific grinding energy (U)

Specific energy U ( $J/mm^3$ ) is one of the important grindability indices. It is calculated as given in equation (1)

$$U = \frac{P}{MRR} = \frac{F_t \times V_c}{b \times a_e \times t} \tag{1}$$

Where  $P$  is the grinding power (Watt),  $MRR$  is the material removal rate ( $mm^3$ ),  $F_t$  is tangential force (N),  $V_c$  is cutting velocity (m/s),  $b$  is the wheel width i.e., 13 mm in this investigation and  $a_e$  is the radial depth of cut ( $\mu$ m) and  $t$  is the table speed (m/min).

As the radial depth of cut increases, there is a reduction in specific energy with various cutting velocities. This can be attributed to the fact that the

rubbing and ploughing action decreases as the radial depth of cut increases, leading to more material removal with most of the energy spend on shearing of material leading to lower specific energy as shown in Fig. 10 (a), (b).

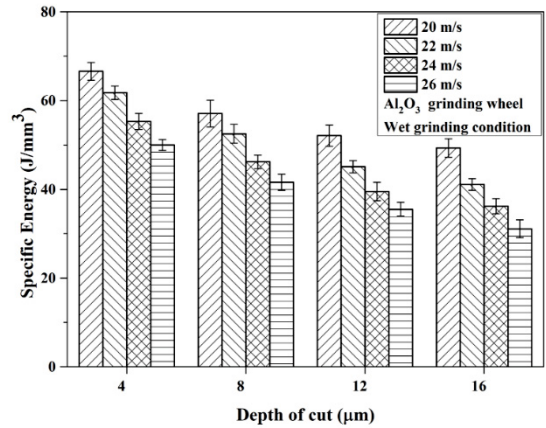


Fig. 10. (a) Variation of specific energy with different process conditions for the Al<sub>2</sub>O<sub>3</sub> wheel.

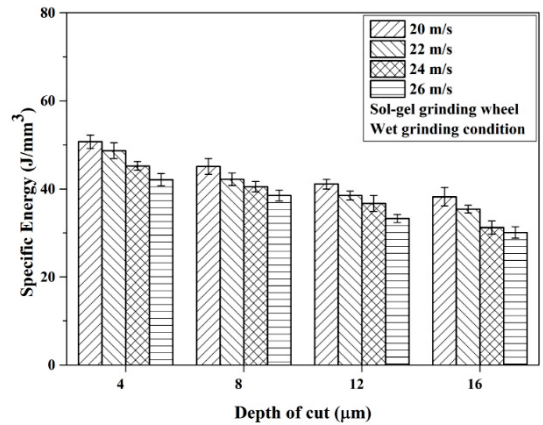


Fig. 10. (b) Variation of specific energy with different process conditions for the sol-gel wheel.

The order of specific energy requirement for the Sol-gel wheel is 21% lower than the alumina due to the cutting edge properties which are related to the tribological behavior during the fine grinding process. The improved cutting and tribological behavior of sol-gel grains were characterized by the greater ductility, which leads to a high resistance to brittle fracture. This increased fracture toughness and ability to fracture at a controlled rate at the sub-micron level, constantly creating thousands of new cutting points contributes to sustained grinding action with lower specific cutting energy [8].

The edge of cutting grits of alumina grinding wheel was subjected to plastic deformation under the effect of strain and temperature. This created a flat contact with the workpiece material. Further, it will cause the force and energy required to increase. The excellent cutting ability of the microcrystalline grains can also be explained by the stable conditions of slippage on flat grain surfaces, created behind the cutting edges.

### 3.5 Chip morphology

SEM images of the chip morphology generated by grinding with both Al<sub>2</sub>O<sub>3</sub> and Sol-gel wheels are provided in Fig. 11 (a), (b) respectively.

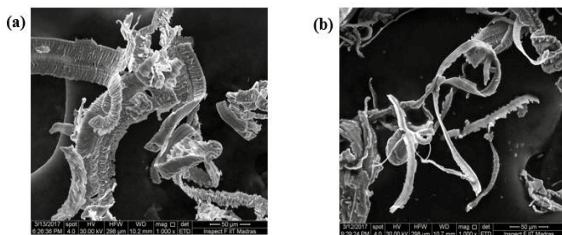


Fig. 11. Typical micrographs of chips ground with (a) Al<sub>2</sub>O<sub>3</sub> and (b) Sol-gel wheel under grinding conditions ( $V_c=26$  m/s,  $a_e=16$   $\mu$ m).

The chip morphology produced by the alumina grinding wheel was short and wide. The chips differ in their form. This can be explained by the irregular cutting effort along the circumference of the grinding wheel with separate working grains. Lot of segmented and split chips were observed with white alumina grinding wheel due to severe plastic deformation. The loss of sharpness in the cutting edges due to the wear and loading in grinding wheel leads to high forces and temperature contributed to the above-mentioned chip morphology. The chips produced when using the sol-gel alumina grinding wheel is continuous and thin with fewer strains on it. This may be due to the grinding action of sol-gel grains which could able to retain the grinding action with the microfracture characteristics of the grains.

### 3.6 Maximum undeformed chip thickness ( $h_m$ )

The specific energy  $U$  (J/mm<sup>3</sup>) is calculated using equation (1). Undeformed chip thickness was used to calculate the specific energy of the grinding process. The maximum chip thickness [1] can be calculated using the following equation:

$$h_m = \left( \frac{3}{c \times \tan \theta} \right)^{1/2} \left( \frac{v_w}{v_c} \right)^{1/2} \left( \frac{a_e}{d} \right)^{1/4} \quad (2)$$

where  $c$  is the active number of grits ( $c$  is 8 from the experimental data),  $\theta$  is the semi-included angle of the chip cross section (assumed to be triangle,  $\theta$  is 60 deg),  $v_c$  is the wheel speed,  $v_w$  is the workpiece speed,  $a_e$  is the radial depth of cut, and  $d$  is the diameter of the grinding wheel. The influence of undeformed chip thickness  $h_m$  with the grinding specific energy of Al<sub>2</sub>O<sub>3</sub> grinding wheel and sol-gel grinding wheel is shown in Fig. 12 (a), (b). The specific energy decreased with increase in the  $h_m$  value for the sol-gel grinding wheel, which indicated that the material removal rate was higher in the absence of wheel loading. Also for the Al<sub>2</sub>O<sub>3</sub> wheel, the specific energy decreases with a higher order value of undeformed chip thickness. This was due to the wheel loading that occurred on the surface of the conventional Al<sub>2</sub>O<sub>3</sub> grinding wheel. The dense sol-gel wheel grains with high fracture toughness leads to sustained sharpness performed well compared to the Al<sub>2</sub>O<sub>3</sub> wheel.

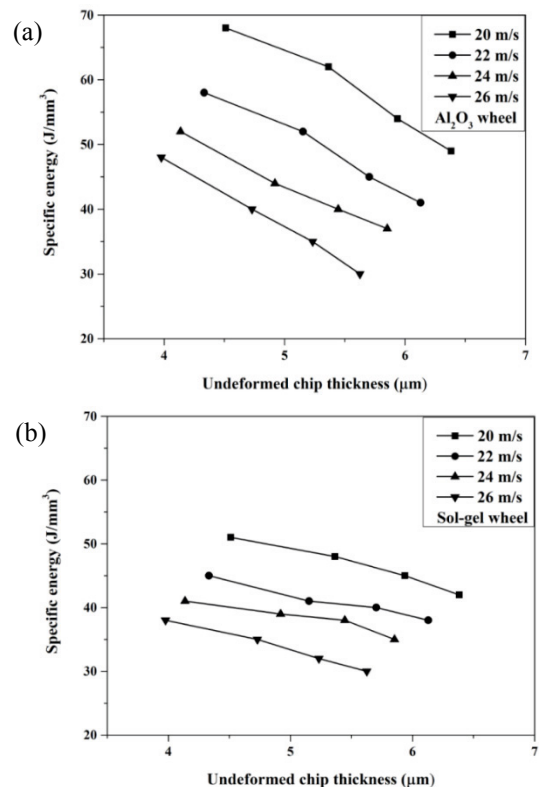


Fig. 12. Variation of undeformed chip thickness with specific energy for various cutting velocities for (a) Al<sub>2</sub>O<sub>3</sub> wheel, (b) sol-gel wheel

### 3.7 Wheel wear assessment

The wheel wear assessment was carried out for both sol-gel alumina grinding wheel and white alumina wheel at constant grinding conditions (cutting velocity at 25 m/s, feed at 9 m/min and depth of cut at 10 μm). Both the grinding wheels were used up to 1000 passes to have an appreciable wear without dressing the grinding wheel. The tests were conducted with selected parameters to evaluate the wear performance of both the grinding wheels. The force plots are shown in Fig. 13 (a), (b). The normal and the tangential forces increase with the number of passes for the grinding wheels. But in the case of the sol-gel grinding wheel sintered at higher temperatures, the forces were lower.

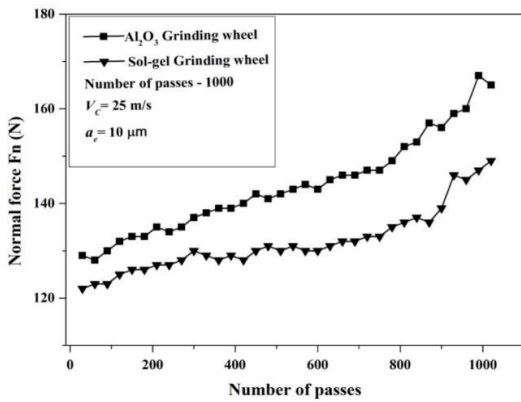


Fig. 13. (a) Variation of number of grinding passes on the Normal force ( $V_c = 25\text{m/s}$ ,  $a_e = 10\mu\text{m}$ ) for  $\text{Al}_2\text{O}_3$  and Sol-gel wheel

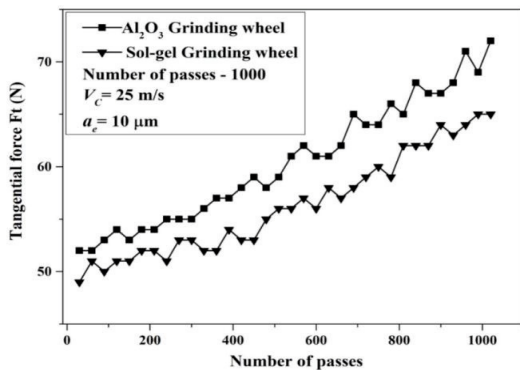


Fig. 13. (b) Variation of number of grinding passes on the normal force ( $V_c = 25\text{m/s}$ ,  $a_e = 10\mu\text{m}$ ) for  $\text{Al}_2\text{O}_3$  and Sol-gel wheel

It may be due to the reduction in wheel loading with an increased self-sharpening action of the abrasive grains. A stereomicroscope was used to capture the images of the grinding wheel, where the brighter area refers to the active cutting edges and the black area refers to the loaded material. The surfaces of the  $\text{Al}_2\text{O}_3$  wheel and sol-gel grinding wheel are shown in Fig. 14 (a, b).

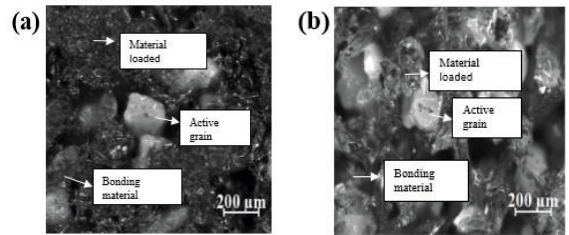


Fig. 14. Wheel loaded images of (a)  $\text{Al}_2\text{O}_3$  and (b) Sol-gel wheel without dressing after 1000 passes under ( $V_c = 25\text{m/s}$ ,  $a_e = 10\mu\text{m}$ ).

It can be observed that the sol-gel wheel has less wheel loading and has more cutting edges compared to the  $\text{Al}_2\text{O}_3$  wheel. This shows that sol-gel wheel has more number of effective cutting edges than the  $\text{Al}_2\text{O}_3$  grinding wheel.

### 3.8 Grinding ratio (G)

The G-Ratio is a reliable index of the wheel wear rate. In order to evaluate the G-Ratio for the various grinding wheels, experiments were performed by grinding the work material up to 1000 passes and keeping only half the wheel in contact with the work material. The cutting velocity was maintained at 25 m/s and depth of cut was 10 μm. Grinding ratio is the ratio of the volume of work material removed to the volume of wheel wear. Wheel wear was measured using a coordinate measuring machine of 0.1 μm resolution. Fig. 15 shows the comparison of G-ratio for  $\text{Al}_2\text{O}_3$  and sol-gel grinding wheels.

It is observed that sol-gel grinding wheel is performing better than the  $\text{Al}_2\text{O}_3$  wheel. The sol-gel grains have higher fracture toughness and micro-fracturing capability leading to the domination of material deformation throughout the grinding process. Therefore, giving rise to a higher order G- Ratio.

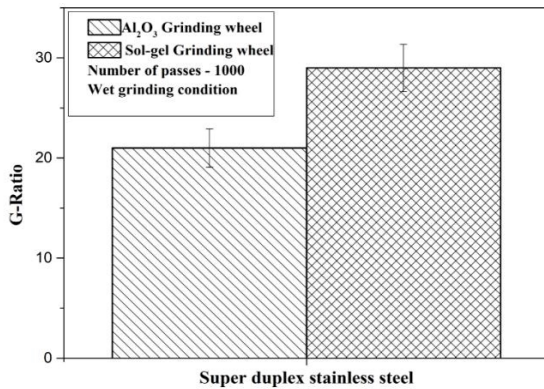


Fig. 15. Comparison of G-Ratio for Al<sub>2</sub>O<sub>3</sub> and sol-gel wheel.

### 3.9 Grinding efficiency (E)

The G-ratio divided by the specific energy is expressed as the grinding efficiency (mm<sup>3</sup>/J/sec) [12]. The grinding efficiency can be increased with an increase in the G-ratio or decrease in the specific energy. The grinding efficiency is given as

$$E = \frac{G}{U} \quad (3)$$

In this equation,  $G$  is defined as the volume of material removed per unit volume of wheel wear and  $U$  (J/mm<sup>3</sup>) is the specific energy. The  $G$  value increases with less wheel wear and/or higher metal removal. The higher  $G$  value indicates a longer wheel life. The grinding ratio  $G$  is defined as

$$G = \frac{V_m}{V_s} \quad (4)$$

where  $V_m$  = Volume of metal removed (mm<sup>3</sup>) and  $V_s$  = Volume of wheel wear (mm<sup>3</sup>). The calculated grinding efficiency for the chosen processing conditions is shown in Fig. 16.

The sol-gel wheel grinding efficiency is much better in comparison with the white alumina wheel. This is due to the following reasons;

- The high fracture toughness properties of the sol-gel grains resulted in a sustained grinding action which leads to a high volume of material removal with less wheel wear.
- The better tribological properties of the sol-gel grains due to their sub-microcrystalline structure and micro fracturing capability makes them more

durable, and maintain their shape longer than those made from white fused alumina [9].

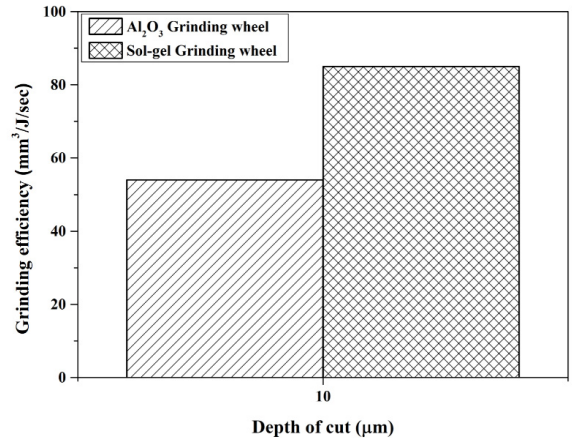


Fig. 16. Grinding efficiency for Al<sub>2</sub>O<sub>3</sub> and sol-gel wheel.

## 4. Conclusion

The sol-gel grinding wheel outperformed the white alumina grinding wheel in all the aspects of performance indices calculated. Based on the observations, following conclusions can be made;

- The sol-gel grinding wheel has shown around 21% reduction in cutting forces and specific cutting energy.
- The average surface finish of the component produced by the sol-gel wheel for the selected processing conditions was shown 27% improvement over the wheel with conventional grains.
- The grinding ratio of the sol-gel alumina grinding wheel showed around 20% increase in comparison with white alumina wheel.
- Overall the grinding efficiency of the sol-gel grinding wheel was around 31% more than the conventional white alumina wheel.

The average crystal sizes of sol-gel abrasives are in sub-micrometer range. The properties of sol-gel abrasive contain high fracture toughness and micro fracture characteristics, which helps in better grinding performance for different applications. Overall the results indicate that sol-gel alumina wheel retains its grain sharpness for longer grinding duration compared to white alumina wheel. The sol-gel grinding wheel can be a potential tool for processing of hard and tough SDSS material.

## References

- [1] Malkin, S., and Guo, C., 2008, *Grinding Technology: Theory and Application of Machining With Abrasives*, Industrial Press, New York.
- [2] Krell, A., Blank, P., Wagner, E., Bartels, G., 1996, Advances in the Grinding Efficiency of Sintered Alumina Abrasives, *Journal of the American Ceramic Society*, Vol. 79, No. 3, p. 763-769.
- [3] S. C. Yoon & M. Krueger, Optimizing grinding performance by the use of sol-gel alumina abrasive wheels and a new type of aqueous metalworking fluid, *Machining Science and Technology*, Vol.3 No.2, 1999,287-294.
- [4] Klocke F., Engelhorn R., Mayer J., Weirich T (2002) Micro-analysis of the contact zone of tribologically loaded second-phase reinforced Sol-gel-abrasives. *CIRP Ann* 51(1):245–250.
- [5] Eduardo Carlos Bianchia, Eraldo Jannone da Silvad, Vinicio Lucas Vargasc, Thiago Cardoso Magagninc, Rodrigo Daun Monicib, Osmar Vicari Filhob, Paulo Roberto de Aguiara, The Grinding Wheel Performance in the Transverse Cylindrical Grinding of an Eutetic Alloy, *Journal of Material Research*, Vol. 5, No. 4, ( 2002) 433-438.
- [6] Mayer J., Engelhorn R., Bot R., Weirich T., Herwartz C., Klocke F (2006) Wear characteristics of second-phase-reinforced sol-gel corundum abrasives. *Acta Mater* 54(13):3605–3615.
- [7] G. Manimaran., M. Pradeep kumar., Effect of cryogenic cooling and sol-gel alumina wheel on grinding performance of AISI 316 stainless steel, *Arch. Civ. Mech. Eng.* 13, September (2013) 304–312.
- [8] Krzysztof Nadolny., State of the art in production, properties and applications of the microcrystalline sintered corundum abrasive grains, *International Journal of Advanced Manufacturing Technol* (2014) 74:1445–1457.
- [9] Krzysztof Nadolny., Wear phenomena of grinding wheels with sol-gel alumina abrasive grains and glass-ceramic vitrified bond during internal cylindrical traverse grinding of 100Cr6 steel, *International Journal of Advanced Manufacturing Technology*, Vol.77, Issue 1, (2015),83-98.
- [10] J Rajaguru ., N Arunachalam., Coated tool Performance in Dry Turning of Super Duplex Stainless Steel, *Procedia Manufacturing* 10,(2017),601–611.
- [11] Stephane Lachance, Robert Bauer, Andrew Warkentin, Application of region growing method to evaluate the surface condition of grinding wheels, *International Journal of Machine Tools & Manufacture*, 44 (2004) 823–829.
- [12]. Patricia L. Smith, A killer combination for ideal grinding conditions, *American machinist*, 1998.